Hydrodynamic Forces on Macromolecules Protruding from Lipid Bilayers Due to External Liquid Flows.

Jönsson, Peter; Jönsson, Bengt

Published in:
Langmuir

DOI:
10.1021/acs.langmuir.5b03421

2015

Document Version:
Peer reviewed version (aka post-print)

Hydrodynamic forces on macromolecules protruding from lipid bilayers due to external liquid flows

Peter Jönsson and Bengt Jönsson*[‡]

Division of Physical Chemistry, Lund University, SE-22100 Lund, Sweden

[‡]Division of Biophysical Chemistry, Lund University, SE-22100 Lund, Sweden

*Correspondence: peter.jonsson@fkem1.lu.se

ABSTRACT: It has previously been observed that an externally applied hydrodynamic shear flow above a fluid lipid bilayer can change the local concentration of macromolecules that are associated with the lipid bilayer. The external liquid flow results in a hydrodynamic force on molecules protruding from the lipid bilayer, causing them to move in the direction of the flow. However, there has been no quantitative study about the magnitude of these forces. We here use finite element simulations to investigate how the magnitude of the external hydrodynamic forces varies with the size and shape of the studied macromolecule. The simulations show that the hydrodynamic force is proportional to the effective hydrodynamic area of the studied molecule, A_{hydro}, multiplied by the mean hydrodynamic shear stress acting on the membrane surface, σ_{hydro}. The parameter A_{hydro} depends on the size and shape of the studied macromolecule above the lipid bilayer and scales with the cross-sectional area of the molecule. We also investigate how hydrodynamic shielding from other surrounding macromolecules decreases A_{hydro} when the surface coverage of the shielding macromolecules increases. Experiments where the protein streptavidin is anchored to a supported lipid bilayer on the floor of a microfluidic channel were finally performed at three different surface concentrations, Φ = 1%, 6%, and 10%, where the protein is being moved relative to the lipid bilayer by a liquid flow through the channel. From photobleaching measurements of fluorescently labeled streptavidin we found the experimental drift data to be within good accuracy of the simulated results, less than 12% difference, indicating the validity of the results obtained from the simulations. In addition to giving a deeper insight into how a liquid flow can affect membrane-associated molecules in a lipid bilayer, we also see an interesting potential of using hydrodynamic flow experiments together with the obtained results to study the size and the intermolecular forces between macromolecules in membranes and lipid bilayers.

INTRODUCTION

A vital property of the membrane that surrounds a living cell is the lateral mobility of proteins and other molecules that are associated with the fluid lipid bilayer that constitutes one of the basic building blocks of the cell membrane.[1] This property is essential for newly synthesized proteins to spread on the cell surface and for receptors and other membrane proteins to move and interact with other molecules therein. The net motion of these macromolecules will without active processes be random and the molecules will due to the laws of diffusion distribute evenly within a corral or enclosure in the membrane.[2,3] How the properties of the macromolecules and the membrane can be used to theoretically predict the free diffusion of these molecules has previously been thoroughly investigated.[3–5] However, it has recently been observed that hydrodynamic forces from a constant liquid flow outside a cell can shift the distribution of macromolecules on the cell surface.[6,7] The reason for this redistribution is that molecules protruding from the lipid bilayer will experience drag forces from the liquid flow above the surface, causing the mobile molecules to move in the fluid lipid bilayer in the direction of the hydrodynamic flow.

This interesting phenomenon has also been observed, and investigated, in more detail in various supported lipid bilayer (SLB) systems. SLBs are common model systems of the cell membrane and consists of a lipid bilayer adsorbed on, typically a glass surface.[8–10] Here different macromolecules including lipids with modified head groups,[11–15] lipid vesicles,[16] bound proteins,[11,13,17] and DNA[18,19] have been transported in the direction of the flow, resulting in a varying concentration of the studied molecules over the lipid bilayer. Figure 1A shows a schematic illustration of an SLB with anchored macromolecules protruding from the SLB under the influence of an external liquid flow. The lipids in the upper monolayer move with a velocity

v_{lipids} due to hydrodynamic shear forces transmitted from the liquid flow. It has previously been shown that the SLB moves in a rolling motion, with the lowest monolayer being essentially stationary, due to the strong coupling between the lower monolayer and the support.[12] The hydrophilic part of the protruding macromolecules will be equivalent to a hydrodynamic sail and will generally cause these macromolecules to move at a higher velocity, $v_{macromolecule}$, than the lipids.[17] If there is a boundary in the SLB, this will result in a redistribution of the protruding macromolecules, with a higher concentration of the macromolecules at the side of the enclosure where the liquid flow is directed (see Fig. 1B).

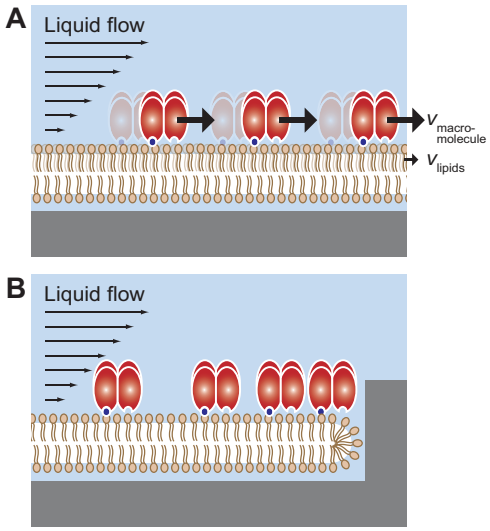

Figure 1. (A) Schematic illustrations showing protruding macromolecules being moved along an SLB by a liquid flow above the lipid bilayer. **(B)** If there is an enclosure or boundary in the lipid bilayer, this results in a redistribution of the macromolecules along the flow direction.

The reduced complexity of SLBs, compared with the cell membrane that surrounds a living cell, together with the possibility to have well-controlled flows above the SLB, opens up for

accurate studies of the hydrodynamic forces that acts on different types of membrane-associated macromolecules. These experiments have indicated that the hydrodynamic drag force on different types of macromolecules anchored to an SLB depends on parameters such as the size and height-to-width ratio of the studied macromolecule as well as the surface coverage of the molecules. However, no detailed theoretical analysis has, to the best of our knowledge, been performed that describes the connection between these parameters and the observed behavior of the hydrodynamic forces on the membrane-associated macromolecules. Such expressions are important in order to understand the conditions that are required to result in a significant redistribution of membrane-associated macromolecules under hydrodynamic flow. It could also make it possible to obtain new information about intermolecular interactions between membrane-associated macromolecules by relating the hydrodynamic force from the liquid flow to the intermolecular forces between the macromolecules.

We have in this work investigated how an externally applied shear flow above an SLB induces hydrodynamic forces on macromolecules that are anchored to the lipid bilayer. This was achieved using finite element simulations where we have modeled the hydrodynamic force for various simplified macromolecule models. The first model system studied consists of a spherical molecule in an infinitely dilute system (see Fig. 2A). This system has previously been thoroughly investigated theoretically[20–22] and was used as a first test to validate the simulations. In the next situation we investigate the influence the shape of the macromolecule has on the hydrodynamic force. This was done by simulating the hydrodynamic flow around cylindrical molecules with different height-to-width ratio (see Fig. 2B). In the last scenario we investigate what happens at higher surface coverage when the molecules start to shield each other from the hydrodynamic

flow (see Fig. 2C). The molecules are assumed to be randomly distributed, which is modeled using a cylindrical unit cell with the radius

$$L = a/\sqrt{\Phi} \tag{1}$$

where a is the cross-sectional radius of the studied macromolecule and Φ is the surface coverage of macromolecules in the lipid bilayer. On the basis of these values, we present empirical expressions describing how the force varies with different parameters such as the cross-sectional radius a, the surface coverage Φ, the height-to-width ratio $h_c/2a$, and the parameter σ_{hydro} which is the (macroscopic) shear stress on the lipid bilayer in the absence of macromolecules on the surface. We finally performed experiments where the protein streptavidin is anchored to an SLB at the floor of a microfluidic channel, which is acted upon by a liquid flow through the channel. The hydrodynamic shear stress, σ_{hydro}, was determined from the dimensions of the channel and the applied flow rate, and the drift velocity of both the lipids in the SLB and the anchored streptavidin was simultaneously determined using photobleaching measurements with the streptavidin and the lipids labeled with different fluorescent groups. These measurements were performed at three different surface concentrations of streptavidin and were compared to the results obtained from the simulations. We finally discuss the implications these finding might have when describing the drift velocity and reorganization of molecules in SLBs as well as on other lipid bilayer systems and on real cell membranes.

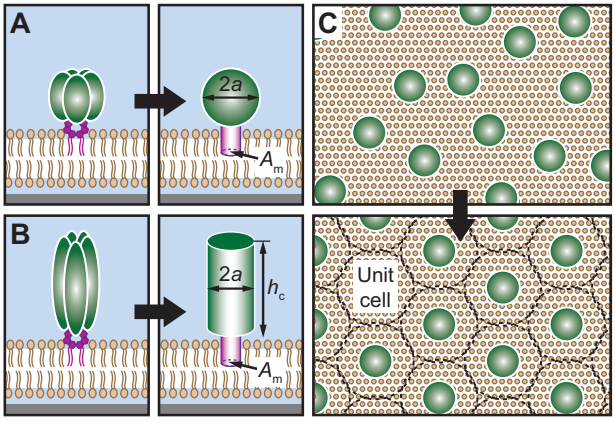

Figure 2. Three different scenarios are considered in this work. In **(A)** we investigate the force on spherical molecules, at infinite dilution. In the next scenario **(B)** we investigate the hydrodynamic force on cylindrical molecules with different height-to-width ratio, $h_c/2a$. In the final case **(C)** we model the effect of hydrodynamic shielding by neighboring macromolecules using cylindrical unit cells (dashed lines) with different radius depending on the surface coverage of molecules.

THEORY

Macroscopic and local flow profiles

It should be noted that even though the main aim with this work is to describe the hydrodynamic force on macromolecules protruding from SLBs, the theoretical discussion in this and the following sections will also be valid for many other lipid bilayer systems as well as real cell membranes. The term "lipid bilayer" is therefore used when the theory applies also to other lipid bilayer systems.

The liquid flow above a lipid bilayer will for most practical cases vary over two different length scales:

- A *macroscopic* length scale over which the lipid bilayer can be considered as a flat, or for cells and lipid vesicles curved, surface where the protruding parts of the individual macromolecules in the lipid bilayer can be neglected.
- A *local* length scale over which the fluid velocity changes around individual macromolecules that are anchored in the lipid bilayer.

For the experiments performed in this work, the macroscopic length scale is of the order of the height of the microfluidic channel, whereas the local length scale is of the order of the size of a streptavidin molecule.

The overall flow velocity $\boldsymbol{u}$ is a sum of the macroscopic and the local velocity contributions, $\boldsymbol{u}_{\text{macro}}$ and $\boldsymbol{u}_{\text{local}}$. The macroscopic velocity is the velocity in the absence of macromolecules protruding from the lipid bilayer, whereas $\boldsymbol{u}_{\text{local}}$ corresponds to the disturbance in the flow profile due to the absorbed molecules. It is therefore the latter velocity which determines the net hydrodynamic force experienced by each macromolecule in the lipid bilayer. Let us now consider the flow over a local area of the lipid bilayer, where the liquid flow above the lipid bilayer is assumed to be in the x-direction:

$$\boldsymbol{u}_{\text{macro}}(z) = \boldsymbol{u}_{\text{lipids}} + \left(z\sigma_{\text{hydro}}/\eta\right)\boldsymbol{e}_x \tag{2}$$

where $\boldsymbol{u}_{\text{lipids}}$ is the local velocity of the lipids (bilayer or monolayer), z is the vertical distance from the surface of the lipid bilayer, η is the viscosity of the liquid, σ_{hydro} is the macroscopic shear stress on the surface and $\boldsymbol{e}_x$ is a unit vector in the x-direction. Thus, the expression in Eq. 2 assumes that the macroscopic velocity increases linearly above the lipid bilayer on a local length scale. This assumption is generally valid for SLBs, where the velocity of the lipid bilayer is orders of magnitude lower than the velocity of the liquid.[23] However, it has also been observed by Honerkamp-Smith et al. to be valid for giant unilamellar vesicles (GUVs) subjected to liquid

flow[24] and could similarly be expected to also hold for many real cell membranes where the frictional coupling between the cytoplasma and the inner monolayer of the cell membrane is substantially larger than for GUVs. The shear stress can vary, macroscopically, on different positions over the surface, but Eq. 2 will in a local sense be valid at all positions. The higher viscosity of the lipid bilayer, compared to the surrounding liquid, will also result in the relative velocity of the macromolecule, v_c, being small compared to the liquid velocity around the molecule: $v_{liquid} \sim h_c \sigma_{hydro}/\eta$, where h_c is the height of the molecule. Thus, the motion of the macromolecules relative to the lipid bilayer is not expected to change the overall flow profile significantly compared to the situation when the macromolecules move with the same velocity as the lipids in the SLB.

The hydrodynamic force, F_{hydro}, experienced by a macromolecule will be proportional to σ_{hydro} according to

$$F_{hydro} = A_{hydro}\sigma_{hydro} \tag{3}$$

where A_{hydro} is a parameter corresponding to the effective hydrodynamic area of the anchored macromolecule above the lipid bilayer. For a molecule with no parts protruding over the lipid bilayer we have $A_{hydro} = A_m$, where A_m is the cross-sectional area of the molecule in the lipid bilayer (see Fig. 2A and B). However, for a macromolecule protruding from the lipid bilayer the effective hydrodynamic area will be larger, and the molecule will therefore experience a greater hydrodynamic force. If the hydrodynamic area is larger than A_m, this means that the macromolecule will move relative to the lipids in the direction of the flow, resulting in a redistribution of the studied macromolecules in the lipid bilayer. It is therefore in most cases the difference $\Delta A_{hydro} = A_{hydro} - A_m$, the excess hydrodynamic area, which is of interest when relating the hydrodynamic force to the relative motion of macromolecules in the lipid bilayer.

Expressions for the hydrodynamic force

Since $\boldsymbol{u}_{\text{local}}$, which gives rise to the net hydrodynamic force, is approximately independent of the lipid velocity as long as Eq. 2 and $v_c < h_c\sigma_{\text{hydro}}/\eta$ holds, as discussed in the previous section, it is convenient to approximate the lipid bilayer as a rigid surface with a stationary, absorbed macromolecule, to determine the hydrodynamic force. Considerable work has been done to describe the flow profile around a single spherical molecule at rest in a pure shear flow near a solid wall.[20–22] These studies show that the hydrodynamic area of a spherical molecule in a linear macroscopic shear flow can be written as[22]

$$A_{\text{hydro}} = 6\pi a^2 (l/a) f_s(l/a) \tag{4}$$

where l is the distance from the solid wall to the center of the sphere ($l = a$ for a sphere bound to the solid surface) and f_s is a dimensionless friction factor that varies from $f_s = 1.70$ for $l = a$ to $f_s = 1$ for $l >> a$.[20–22] Equation 4 will in the latter case correspond to the drag force experienced by a sphere at rest in an unbounded shear flow where the macroscopic velocity at the center of the sphere is $l\sigma_{\text{hydro}}/\eta$.

Equation 4 gives a simple description of how the hydrodynamic force on a single spherical macromolecule depends on parameters such as shear strength, molecular size and distance between the molecule and the lipid bilayer. However, the value of f_s for a non-spherical molecule, and how A_{hydro} varies if there is more than one molecule on the surface, is not included in Eq. 4. Instead, Eq. 5 presents a general formula for A_{hydro} for a cylindrical molecule on the surface of a lipid bilayer (see Fig. 2B):

$$A_{\text{hydro}} = 3\pi a^2 (h_c/a) f_c(h_c/a, \Phi) \tag{5}$$

The friction factor f_c will depend on the height-to-width ratio of the cylindrical molecule and the surface coverage of the macromolecules, Φ. The latter arises due to hydrodynamic shielding by neighboring molecules, which can reduce the hydrodynamic force significantly. However, how to choose f_c as a function of h_c/a and Φ is not known. One approximation that has been used at low surface coverage is to replace the parameter a by an effective radius a_{eff} defined as[25]

$$a_{\text{eff}} = \left(\frac{3V}{4\pi}\right)^{1/3} = \left(\frac{3a^2 h_c}{4}\right)^{1/3} \tag{6}$$

where V is the volume of the cylinder and setting $f_c = 1$. However, the accuracy of this approximation has not been tested. Finite element simulations, as described in the next section, where performed to investigate how the effective hydrodynamic area of a macromolecule depends on its height-to-width ratio and the surface coverage of molecules.

MATERIALS AND METHODS

Numerical simulations

Governing equations. In order to investigate how a constant liquid flow above a lipid bilayer acts on macromolecules protruding from the lipid bilayer, we used finite element simulations to solve Navier-Stokes' equations within the creeping flow approximation around two simplified geometrical models of the studied macromolecules: (i) spherical molecules and (ii) cylindrical molecules with different height-to-width ratios, where the molecules are attached to a surface in all cases. It is here also important to point out that it is enough, due to the linearity of the creeping flow equations, to solve for the change in the local velocity $\boldsymbol{u}_{\text{local}}$, instead of the full velocity, $\boldsymbol{u}$ (see the section "Creeping flow equations" in the Supporting Information for details):

$$0 = -\nabla p_{\text{local}} + \eta \nabla^2 \boldsymbol{u}_{\text{local}} \tag{7}$$

$$\nabla \cdot \boldsymbol{u}_{\text{local}} = 0 \tag{8}$$

where $\boldsymbol{u}_{\text{local}} = \boldsymbol{u} - \boldsymbol{u}_{\text{lipids}} - (\sigma_{\text{hydro}} z/\eta)\boldsymbol{e}_x$ is the change in the local flow velocity vector and p_{local} the change in the local pressure compared to the situation with a flat surface without macromolecules. This facilitates the convergence of the simulations considerably. Both $\boldsymbol{u}_{\text{local}}$ and p_{local} will scale linearly with σ_{hydro}. Furthermore, the value of the hydrodynamic force will be proportional to the cross-sectional area of the macromolecule for two macromolecules with the same shape and the same surface coverage (see the section "Creeping flow equations" in the Supporting Information for details). Thus, it is sufficient to perform the simulations for one hydrodynamic shear stress, and one size, for the different types of macromolecules studied.

Finite element simulations. Equations 7 and 8 were solved using the *Creeping flow module* in COMSOL Multiphysics® 4.3b (COMSOL AB, Sweden) to obtain $\boldsymbol{u}_{\text{local}}$ and p_{local}. The hydrodynamic drag force in the x-direction (the direction of the liquid flow) was obtained by integrating

$$dF_x = \left(p_{\text{local}} - 2\eta \frac{\partial u}{\partial x} \right) n_x dA - \eta \left(\frac{\partial u}{\partial y} + \frac{\partial v}{\partial x} \right) n_y dA - \eta \left(\frac{\partial u}{\partial z} + \frac{\partial w}{\partial x} \right) n_z dA - \sigma_{\text{hydro}} n_z dA \tag{9}$$

where dF_x is the hydrodynamic drag force on a part of the macromolecule with the area dA, $\boldsymbol{n} = (n_x, n_y, n_z)$ is the unit normal vector and $\boldsymbol{u}_{\text{local}} = (u, v, w)$ is the local velocity of the liquid.[26]

The simulation geometry consisted of a cylindrical unit cell as shown in Fig. 3, where the radius of the unit cell, L, was defined by Eq. 1. The height of the unit cell was chosen as $1.5L + 2h_c$. No significant change in the results was obtained by using a higher unit cell. Only a quarter of the cylindrical unit cell needed to be included in the simulations due to symmetry

conditions, which considerably speeded up the calculation time. Figure 3A and B shows the simulation geometry for the spherical model molecules.

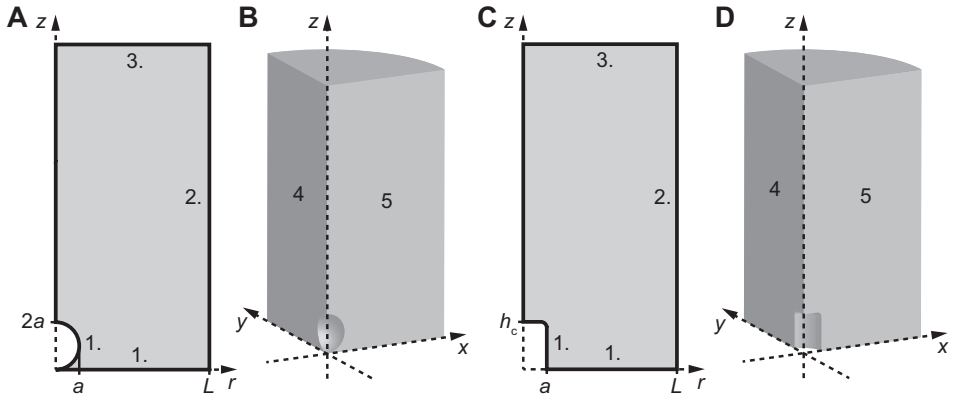

Figure 3. Two different calculation geometries used in the finite element simulations to describe a unit cell with the radius given by the surface coverage of macromolecules according to Eq. 1 with *a* fixed. A solid sphere describes the anchored macromolecule in **(A, B)** and a solid cylinder describes the anchored macromolecule in **(C, D)**. The different numbers in the figures correspond to the boundary conditions used in the simulation (see Table 1).

For the simulations of a cylindrical model molecule (geometry shown in Fig. 3C, D) the top edge of the cylindrical molecule was slightly rounded to avoid the singularity that a profile with a sharp edge produces. This also makes it easier to construct a calculation mesh that can produce accurate results with a minimum of mesh points. Simulations were made where the fillet radius of the edge was *a*/10 and *a*/20, from which the force for a sharp edge was extrapolated from a linear fit. The boundary conditions used in the simulations are summarized in Table 1. The local velocity, $\boldsymbol{u}_{\text{local}}$, is the velocity difference caused by the adsorbed macromolecule compared to the situation for a flat surface (see Eqs. S3 and S4 in the Supporting Information). The boundary

condition at boundaries 1 thus corresponds to the velocity $\boldsymbol{u} = \boldsymbol{u}_{\text{lipids}}$, i.e. "no slip", and the local velocity varies with z as shown in Table 1.

Table 1. Boundary conditions used for the finite element simulations. Only parameter values not indicated with (-) are included. For numbering of the boundaries see Fig. 3.

	u[a]	v[a]	w[a]	p_{local}
1	$-\sigma_{\text{hydro}}z/\eta$	0	0	-
2	-	-	0	0
3[b]	-	-	-	-
4	-	0	0	0
5[c]	-	0	-	-

[a] The velocity components of the local velocity are $\boldsymbol{u}_{\text{local}} = (u, v, w)$. Note that the local velocity, $\boldsymbol{u}_{\text{local}}$, is the velocity difference compared to the situation without an absorbed macromolecule, i.e. $\boldsymbol{u}_{\text{local}} = \boldsymbol{u} - \boldsymbol{u}_{\text{lipids}} - (\sigma_{\text{hydro}}z/\eta)\boldsymbol{e}_x$.

[b] Zero total stress ($[p_{\text{local}}\mathbf{I} + \eta(\nabla\boldsymbol{u}_{\text{local}} + (\nabla\boldsymbol{u}_{\text{local}})^{\text{T}}]\boldsymbol{n} = 0$).

[c] Symmetry (no normal velocity and no tangential viscous stress).

Both the local pressure and the local velocity will approach zero far from the surface, and at boundary 3 a boundary condition corresponding to zero total stress was chosen. This is equivalent to only having a shear flow far above the lipid bilayer, where the change in the local velocity component is zero. The local velocity in the z-direction, and the local pressure, at the side of the unit cell (boundary 2 in Fig. 3) was chosen to be zero. It might at a first instance seem odd that there is no net pressure gradient across the unit cell, since a pressure gradient is generally the driving force for the macroscopic liquid flow. However, the driving force is here instead a constant shear flow above the surface, equivalent to a no-slip, moving wall a macroscopic distance above the surface. Any changes in the macroscopic pressure across a unit cell can furthermore be shown to be negligible compared to the changes in p_{local} around the

absorbed molecule (see Eq. S6 in the Supporting Information). The boundary conditions at boundaries 4 and 5 in Fig. 3 utilize the symmetry of the system. The boundary conditions on boundaries 2, 4, and 5 would for a full, instead of a quarter, unit cell correspond to periodic boundary conditions on boundary 2.

It can also be discussed whether choosing a cylindrical cell model to describe the average flow profile around a single macromolecule in a random array of molecules is an accurate model. However, spherical or cylindrical unit cells have previously been used to model flow behavior around randomly distributed molecules[27] and can be viewed as providing a first approximation of the flow around the molecules in our system at different surface coverage. This approximation will strictly speaking only be valid at a surface coverage below ~50%. At higher coverage the influence of packing, and the overlap between different unit cells, start to be significant, and the accuracy of the cell model becomes questionable.

Simulations were performed where the surface coverage Φ was varied using a parametric sweep after which the total hydrodynamic force was obtained by integrating Eq. 9 over the surface of the adsorbed molecule (and multiplying by four to account for using a quarter of the entire unit cell). Different ratios h_c/a were investigated for the cylindrical molecules. The radius a was chosen to 2 nm, the viscosity $\eta = 1$ mPa·s, and the shear stress σ_{hydro} = 100 Pa in all simulations.

Experimental materials and methods

Microfluidic channels. 150 μm high and 5 mm wide sticky-Slide microfluidic channels were obtained from Ibidi, Germany (sticky-Slide I 0.1 Luer; the extra 50 μm in height comes from the adhesive layer) and were assembled on a cover glass slide (24×60 mm, nr 1, Menzel-Gläser,

Germany) making up the floor of the channel. The glass slide was first cleaned with piranha solution, a 3:1 by volume mixture of concentrated sulfuric acid (95-97%; Merck, Germany) and 30% hydrogen peroxide (Honeywell Specialty Chemicals, Germany), for 20 minutes under moderate heating. The glass slide was then thoroughly rinsed with Milli Q™ water (Millipore, US) and dried with nitrogen gas before the adhesive channel was assembled with the glass slide. The assembled channel was filled with buffer solution containing 150 mM NaCl (Merck) and 10 mM tris[hydroxymethyl]aminomethane (Trizma; Sigma-Aldrich, Sweden), adjusted to a pH of 8.0, and stored at 4°C between the different experiments.

Formation of supported lipid bilayers. Small unilamellar lipid vesicles were prepared by sonication (10 s pulse/10 s waiting time, for a total of 15 minutes at 50% amplitude; Vibra-Cell tip sonicator, Sonics & Materials Inc., US). The vesicles consisted of 1 palmitoyl-2-oleoyl-*sn*-glycero-3-phosphocholine (POPC) from Avanti Polar Lipids (US) with either (i) 0.1 wt% of Oregon Green® 488 1,2-dihexadecanoyl-*sn*-glycero-3-phosphoethanolamine (OG488-DHPE; Invitrogen, US) or (ii) 2 wt% 1,2-dipalmitoyl-*sn*-glycero-3-phosphoethanolamine-N-(cap biotinyl) (sodium salt) (biotin-PE; Avanti Polar Lipids). An SLB on the floor of the microfluidic channel, the glass slide, was made by mixing vesicles of type i and ii to obtain SLBs of different stochiometric ratios, as previously described by us,[25] and then injecting the vesicle mix in a buffer solution (~50 µg lipids per mL) containing an additional 10 mM $CaCl_2$ (Merck) to facilitate vesicle rupture. After approximately 20 minutes an SLB had formed in the microfluidic channel, and the vesicles in solution were rinsed off. A solution containing 10 µg/mL (~200 nM) of Streptavidin, Alexa Fluor® 647 conjugate (SA-647; Invitrogen), was next injected over the SLB for 30 min before rinsing after which all the biotin binding sites on the SLB was occupied

by SA-647. The surface coverage of SA-647 for the different experiment was determined assuming that an SLB with 0.1 wt% biotin-PE gives a SA-647 surface coverage of 2.84%.[25]

Microscopy setup. The fluorescently-labeled molecules were studied with an inverted Nikon Eclipse TE2000-U microscope (Nikon Corporation, Japan) using a Hamamatsu ORCA-Flash4.0 LT sCMOS camera (Hamamatsu, Japan), and a 60× magnification (CFI Apochromat TIRF, NA = 1.49) oil immersion objective (Nikon Corporation). The acquired images were binned (2×2), resulting in a pixel width of 0.22 μm. For the illumination a 60 mW diode laser from Cobolt, Sweden (MLD, 06-01 series) operating at 488 nm was used to excite the lipids OG488-DHPE, and a 140 mW diode laser from Cobolt (MLD, 06-01 series), operating at 638 nm was used to excite the protruding proteins, SA-647. The emitted light from OG488-DHPE and SA-647 was directed to the left and the right half, respectively, of the sCMOS sensor area using W-VIEW GEMINI Image splitting optics from Hamamatsu. To reduce the effect of fluorescence resonance energy transfer (FRET) on the imaging, the 488 nm laser was turned off when taking a 637 nm image of the SA-647 and vice versa when acquiring a 488 nm image of the OG488-DHPE. This was controlled by a custom-written script in the program Micro-Manager 1.4,[28] which also was used for all image acquisition. By moving the point at which the laser enters the objective, the angle of incidence was adjusted such that the light was totally reflected, and the imaging was in total internal reflection fluorescence (TIRF) mode. The images were typically acquired with an exposure time of 100 ms, and a time between frames of 1-2 s was used for the experiments. All measurements were made at ambient temperature, approximately 22°C.

Drift velocity measurements. Gravity was used to control the flow rate through the channel. A beaker with buffer solution was placed above the channel with a tube leading from the beaker to the inlet of the channel. Another tube was connected from the outlet of the channel to a

measurement cylinder placed below the channel. The flow rate through the channel was approximately 20 mL/min for all experiments but was determined individually for each measurement and was used to normalize the data to 20 mL/min flow. To measure the drift velocity of the molecules in the SLB, a custom-made fluorescence recovery after photobleaching setup was used. This consisted of a motorized flip mount from Thorlabs (Germany) to which an opaque disk with a 1 mm slit was mounted. Bringing the slit in the laser light path resulted in only a line of the sample (field of view) being illuminated. By removing the ND filters in the filter wheel (Thorlabs), the intensity of the laser light was increased a factor of 1000, and the fluorescent molecules were illuminated and photobleached for 1 s. The ND filters when then brought back in place, and the opaque disk with the slit was removed. The two lasers were then alternated such that the 488 nm was first illuminating the sample and then the 638 nm laser in order to minimize the effect of FRET to the 638 nm channel. The images were acquired at 1-2 s intervals.

Analysis of the data. All data were analyzed by a custom-written program in MATLAB 2014a (MathWorks, US). A set of four prebleach images was first acquired, and averaged, and used to compensate for an uneven illumination profile by dividing the subsequent images with the averaged prebleach image (after subtraction of dark counts). A 200 pixel wide strip, perpendicular to the bleached line, was next averaged to a line and used to analyze the drift mobility data. All the line profiles were fitted as a function of distance along the line, x, and time after the first frame, t, to the expression

$$y = p_1 - p_2\sqrt{\frac{p_3^2}{p_3^2 + 4p_4t}}\exp\left(-\frac{(x - p_5 - p_6t)^2}{p_3^2 + 4p_4t}\right) + p_7\sqrt{\frac{p_8^2}{p_8^2 + 4p_9t}}\exp\left(-\frac{(x - p_{10} - p_{11}t)^2}{p_8^2 + 4p_9t}\right) \quad (10)$$

where p_1 to p_{11} were constants to be fitted. For SA-647 p_7 to p_{11} were set to zero, and p_4 then corresponded to the diffusivity of SA-647 and p_6 to the drift velocity. This expression can be shown to be valid when the bleach profile at $t = 0$ is approximately Gaussian, as is the case here, following a procedure similar to that used by Jönsson et al. for radial symmetry.[29] However, for the OG488-DHPE data an extra, positive, Gaussian curve needed to be added due to FRET transfer to the 638 channel at higher concentrations of SA-647. The explanation for this is likely that bleached SA-647, moving faster than the lipids, will not FRET as efficiently as unbleached SA-647, resulting in a higher intensity in front of the bleached lipids in the 488 nm images. Whereas this was observed to make the determination of the diffusivity of the lipids at higher concentrations of SA-647 slightly sensitive to the number of frames analyzed and the fitting procedure, this was not a significant issue for the drift velocity determination.

RESULTS AND DISCUSSION

Hydrodynamic force at low coverage for spherical molecules

The presence of a spherical molecule on the surface changes the local flow profile around the adsorbed macromolecule. Figure 4 shows how the local velocity and pressure components varies around a spherical molecule at low surface coverage where the influence of neighboring molecules on the flow profile is negligible ($\Phi = 0.001$). The molecule is attached to the surface at $z = 0$, and there is a macroscopic liquid flow in the x-direction.

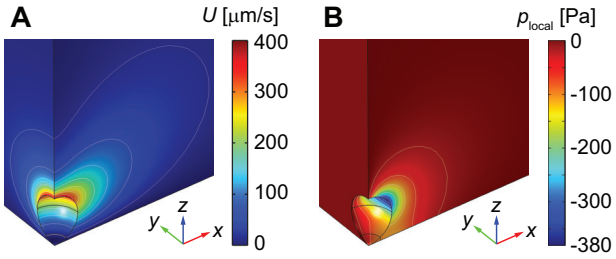

Figure 4. Simulated values showing how the local flow profile varies around the absorbed spherical molecule at low coverage. **(A)** Image showing the magnitude of the local velocity field, $U = (u^2 + v^2 + w^2)^{0.5}$. **(B)** Image showing the local pressure distribution around the molecule. The white lines show contours of constant local velocity and pressure.

From Figure 4 it can be observed that the local flow and pressure profiles that the macroscopic shear flow produce have their maximum values near the top of the protruding molecule. These observations imply that it is this region of the anchored macromolecule that gives the main contribution to the hydrodynamic force that acts on the molecule. By extrapolating the simulated values at low values of Φ to zero surface coverage, we find that the effective hydrodynamic area approaches the value $A_{\mathrm{hydro}}(0) = 10.2\pi a^2$, which from the definition in Eq. 4 gives $f_s = 1.70$. This value is in good agreement with previous theoretical calculations where[20–22]

$$f_s(l/a) \approx 1 + 0.7(l/a)^{-1} \tag{11}$$

Using $f = 1$ to estimate the hydrodynamic force, as is the case for a spherical molecule in solution, will therefore result in a hydrodynamic force that is approximately half the actual value.

The hydrodynamic area can also be viewed as the area on the surface beneath the molecule that is shielded from the external liquid flow (see Fig. S1 in the Supporting Information). This value will always be larger than, or in the limit of thin molecules equal to, the cross-sectional area of

the molecule. For the spherical molecule on the surface this value is 10 times larger than the cross-sectional area of the sphere.

Flow around molecules with different shape

In this section we investigate the effect of the shape of the molecule and for this purpose perform simulations on cylindrical molecules with different height-to-width ratios. Figure S2 in the Supporting Information shows the local flow profile around two cylindrical molecules, one with $h_c = a$ and one with $h_c = 4a$, at a surface coverage $\Phi = 0.001$. The taller molecules experience a higher velocity, and thus also a higher drag force, than the lower molecules. Plotting the hydrodynamic force for different ratios of h_c/a by extrapolating the data to $\Phi = 0$ gives the data points shown in Fig. 5A.

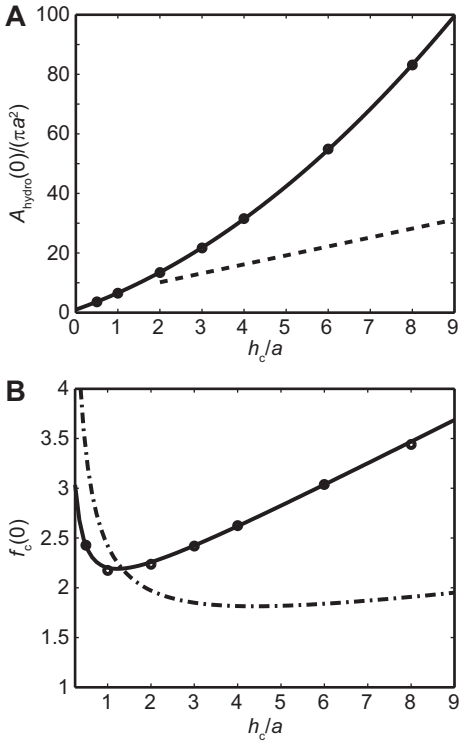

Figure 5. (A) Simulated values for the hydrodynamic force when Φ = 0 (○). The solid line is a quadratic polynomial fit to the simulated data (see Eq. 12). The dashed line corresponds to the theoretical expression in Eq. 4 for a spherical molecule at different distances $l = h_c/2$ from the surface, starting at $l = a$. **(B)** A graph showing the simulated values (○) and the quadratic fit (solid line) in A converted into the parameter f_c defined by Eq. 5. The dot-dashed line is the value of f_c obtained when replacing a with a_{eff} (defined by Eq. 6) in Eq. 5.

The solid line in Fig. 5A is a quadratic polynomial fit yielding

$$A_{\text{hydro}}(0) = \left[0.65(h_c/a)^2 + 5.0(h_c/a) + 1\right]\pi a^2 \tag{12}$$

As the height of the cylindrical molecules gets progressively smaller, the hydrodynamic force approaches the value obtained from the hydrodynamic shear stress on the top of the cylinder. The hydrodynamic drag force increases as the cylinder gets higher. Since both the average flow

velocity around the cylinder and its area scale with the height of the molecule, this results in a $(h_c/a)^2$ dependence of the force at large values of h_c/a. Figure 5 also shows the corresponding value for an anchored spherical molecule. The hydrodynamic area is for this case increasing approximate linearly with ($h_c/a = 2l/a$) and is smaller than the values for the cylinders for all ratios h_c/a.

The data points for A_{hydro} for the cylindrical molecule have in Fig. 5B been used to calculate f_c as defined by Eq. 5. The obtained value is larger than the corresponding value for the spherical molecules, which is 1.7. An explanation to this is the larger area of the cylindrical molecule at the top part of the molecule, where the flow velocity is the highest. The value for f_c increases furthermore linearly with the quotient h_c/a at larger heights of the molecule, as expected from Eq. 12. Figure 5B also shows what the value of f_c should be when replacing a with a_{eff} (given by Eq. 6) in Eq. 5 as has previously been used as an approximation to estimate the hydrodynamic force on a nonspherical molecule.[25] The value of f_c is in this case fairly constant in the interval $h_c/a = 2$ to 8, where it varies between 1.8 and 2.0, which is of the same magnitude as the value of f_c for a spherical molecule. However, the value for f_c will increase drastically at smaller ratios of h_c/a, where the hydrodynamic force approaches the value $\sigma_{hydro}\pi a^2$ (see Eq. 12).

Effect of hydrodynamic shielding

The molecules start to shield each other from the liquid flow when the surface coverage of the molecules increases (see Fig. S3 in the Supporting Information). When the molecules get closer together, the resulting flow approaches that over a flat surface starting at $z = h_c$. The maximum value of the local velocity remains similar to the low coverage case shown in Fig. 4A, but the gradient in the velocity outside the surface of the sphere is changing slower compared to at

$\Phi = 0.001$. The local pressure is also reduced at higher coverage. This is due to shielding of the flow from neighboring molecules which has the effect of lowering the hydrodynamic force per molecule. This can also be stated as the shielded surface area beneath each molecule being reduced due to overlap with the shielded surface area of neighboring molecules (cf. Fig. S1 in the Supporting Information). The latter makes it possible to predict how A_{hydro} will behave at high surface coverage:

$$A_{\mathrm{hydro}}(\Phi \to 1) = \pi a^2 / \Phi \tag{13}$$

since the entire hydrodynamic force from the liquid flow is taken up by attached molecules in this case. The transition from low to high coverage can similarly be argued to start around $\Phi \sim \pi a^2 / A_{\mathrm{hydro}}(0)$, which corresponds to a unit cell having the same area as the value of A_{hydro} for low coverage. From Eq. 12 we know that $A_{\mathrm{hydro}}(0)$ increases with the height-to-width ratio of the molecule, which also means that molecules with a large ratio h_c/a will start to shield each other at lower coverage than is the case for shorter molecules. The values for the hydrodynamic area as a function of surface coverage are shown in Fig. 6A for spherical molecules and in Fig. 6B for cylindrical molecules with different height-to-width ratios (see also Table S1 in the Supporting Information for a list of values). Only data points up to $\Phi = 0.5$ were included since the assumptions made in the cell model are questionable at higher surface coverage. However, Eq. 13 is still expected to hold for higher surface coverage even if the bound molecules are not randomly distributed.

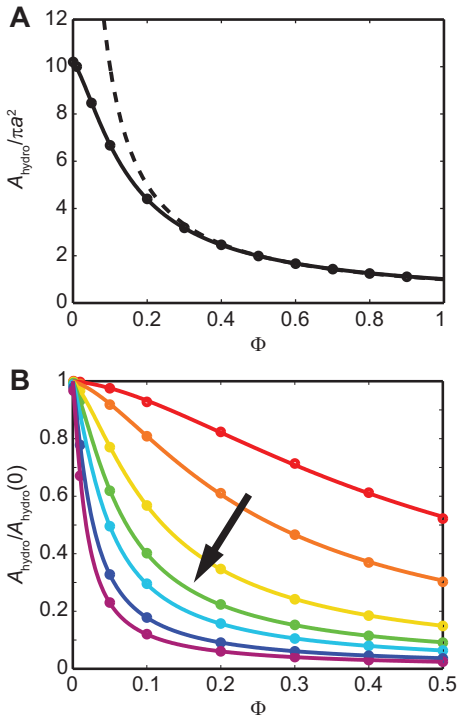

Figure 6. (A) Simulated values (○) showing how A_{hydro} varies with the surface coverage of adsorbed, spherical molecules together with a fit of the data to Eq. 14 (solid line). The dashed line corresponds to the expression 1/Φ. **(B)** Simulated values (○) for cylindrical molecules with different ratios h_c/a as a function of surface coverage (h_c/a = 0.5, 1, 2, 3, 4, 6, and 8; the arrow is in the direction of increasing h_c/a). The data are normalized to $A_{\text{hydro}}(0)$. The solid lines correspond to the empirical expression given by Eq. 14.

The simulated data in Fig. 7 was fitted to the rational function

$$\frac{A_{\text{hydro}}(\Phi)}{A_{\text{hydro}}(0)} = \frac{C_1(h_c/a) + \Phi' C_2(h_c/a)/C_1(h_c/a)}{C_1(h_c/a) + \Phi' C_2(h_c/a) + \Phi'^2 C_2(h_c/a)/C_1(h_c/a)} \tag{14}$$

where

$$\Phi' = \Phi A_{\text{hydro}}(0)/\pi a^2 \tag{15}$$

and

$$C_1(h_c/a) = 1.1 + 0.090(h_c/a) \tag{16}$$

$$C_2(h_c/a) = \frac{1 + 2.1(h_c/a)}{2.9 + (h_c/a)} \tag{17}$$

The coefficients C_1 and C_2 were obtained from a global fit of the data and only depend on the ratio h_c/a. The expression in Eq. 14 was empirically chosen as a relatively simple function that can be used to describe all simulated observations with a correct behavior for both large and small values of Φ. However, Eq. 14 should only be considered as an aid in estimating the effect of hydrodynamic shielding on different systems. When the molecules get closer, at a coverage around $\Phi \sim \pi a^2/A_{\text{hydro}}(0)$, they will start to interfere with the flow profile around neighboring molecules, thus resulting in a decrease in the hydrodynamic force per molecule (see also the definition of Φ′ in Eq. 14). At higher coverage the molecules will already be shielded from each other, and a change in Φ will only result in a modest change in the hydrodynamic force according to Eq. 13 (see also the dashed line in Fig. 6A). For the spherical molecule the coefficients C_1 and C_2 take on the values C_1 = 1.3 and C_2 = 1.1, similar to the values for a cylindrical molecule with $h_c = 2a$. However, it should be noted that Eq. 14 is only a simplified equation to aid in the understanding of how the hydrodynamic force changes with Φ. Since we already have an expression for the force at large Φ, we here focus on the behavior at small to moderate surface coverage, which is also the regime where the cell model approximation holds best. The empirical formula in Eq. 14 gives an estimate of the hydrodynamic force acting on the molecules at different surface coverage, which is generally accurate to within 1% over the investigated range.

Redistribution of molecules in a lipid bilayer

The hydrodynamic force can be converted into a hydrodynamic free energy difference of the studied macromolecules, ΔG_{hydro}:

$$\Delta G_{\text{hydro}} \approx F_{\text{hydro}} d \tag{18}$$

where d is the length scale over which the force is acting, for example the size of a cell or an enclosure in the lipid bilayer. The hydrodynamic force a membrane-anchored macromolecule will experience from a hydrodynamic flow will dominate over diffusion when the hydrodynamic free energy difference, ΔG_{hydro}, is larger than $k_{\text{B}}T$. The distance where $\Delta G_{\text{hydro}} = k_{\text{B}}T$ will correspond to a characteristic distance, which we call the hydrodynamic length, d_{hydro}. An external liquid flow will have a significant effect on the distribution of macromolecules within an enclosure, or over an entire cell, as long as the size of the enclosure, or cell, is larger than d_{hydro}.

For the nonequilibrium situation when the studied macromolecules have just started to be transported by the hydrodynamic force, this will result in a net velocity of the molecules, v_{c}, relative to the lipid bilayer. This velocity results from a balance of the hydrodynamic force, F_{hydro}, with frictional forces from within the lipid bilayer. The latter forces will increase with v_{c}, but the exact form of this dependence will vary with the studied system. A useful approximation for many situations is given by Eq. 19, which utilizes the Einstein relation[30] between the mobility and the diffusivity of the studied molecule in a lipid bilayer to arrive at

$$F_{\text{hydro}} - A_{\text{m}}\sigma_{\text{hydro}} \approx v_{\text{c}} k_{\text{B}}T / D_{\text{c}} \tag{19}$$

where k_{B} is Boltzmann's constant, T is the temperature, and D_{c} is the diffusivity of the macromolecule in the lipid bilayer. Equation 19 is approximately valid for the following two situations:

- When a macromolecule is anchored to the upper monolayer of an SLB.

- When the two monolayers in the lipid bilayer are moving with approximately the same velocity and where the diffusivity is mainly given by frictional drag within the lipid bilayer.

The term $A_m\sigma_{hydro}$ has been included in the left expression in Eq. 19 to account for the effect of displacing lipids in the lipid bilayer when the macromolecule moves. This can equivalently be stated as the net hydrodynamic force being given by $\Delta A_{hydro}\sigma_{hydro}$. However, the term $A_m\sigma_{hydro}$ can often be neglected for larger macromolecules.

The properties of the lipid bilayer will affect the drift velocity of the macromolecules but will not significantly affect the external hydrodynamic force experienced by the macromolecule. By knowing the drag coefficient of the macromolecule in the lipid bilayer, either from experimental measurements[31–34] or from theory[3–5], this makes it possible to determine the relative velocity of the macromolecule compared to the lipids even if the lipids have a none negligible velocity.

The above discussion can also be viewed in terms of the Péclet number, Pe, which is the ratio between the advective transport rate and the diffusive transport rate in the system, which with the definitions used previously gives

$$\mathrm{Pe}=dv_c/D_c \tag{20}$$

Inserting the expressions in Eqs. 18 and 19 into Eq. 20 with $d = d_{hydro}$ results in Pe = 1; thus, the distance d_{hydro} corresponds to the distance where the advective transport rate equals the diffusive transport rate.

Experimentally measured drift velocities

SLBs containing fluorescently-labeled lipids, OG488-DHPE, and the labeled protein streptavidin, SA-647, were made on the floor of a microfluidic channel at three different surface

coverage of SA-647. Applying a flow rate of 20 mL/min in the channel resulted in a hydrodynamic shear stress σ_{hydro} = 18.1 Pa in the center of the channel,[35] moving the lipids and the proteins in the direction of the flow. Photobleaching a line perpendicular to the flow direction allowed for the simultaneous determination of the drift velocity of SA-647 and the lipids OG488-DHPE as well as their diffusivities. Figure 7A shows an image of the fluorescent lipids (left) and streptavidin (right) just after photobleaching and then at intervals of 10 s at a SA-647 surface coverage of Φ = 1.2%. Corresponding intensity line profiles are shown in Fig. 7B, whereas Fig. 7C shows intensity line profiles at Φ = 10.3%. The solid lines in all of the line profiles are curve fits to Eq. 10. Table 2 summarizes the result of these fits at the three different surface coverages.

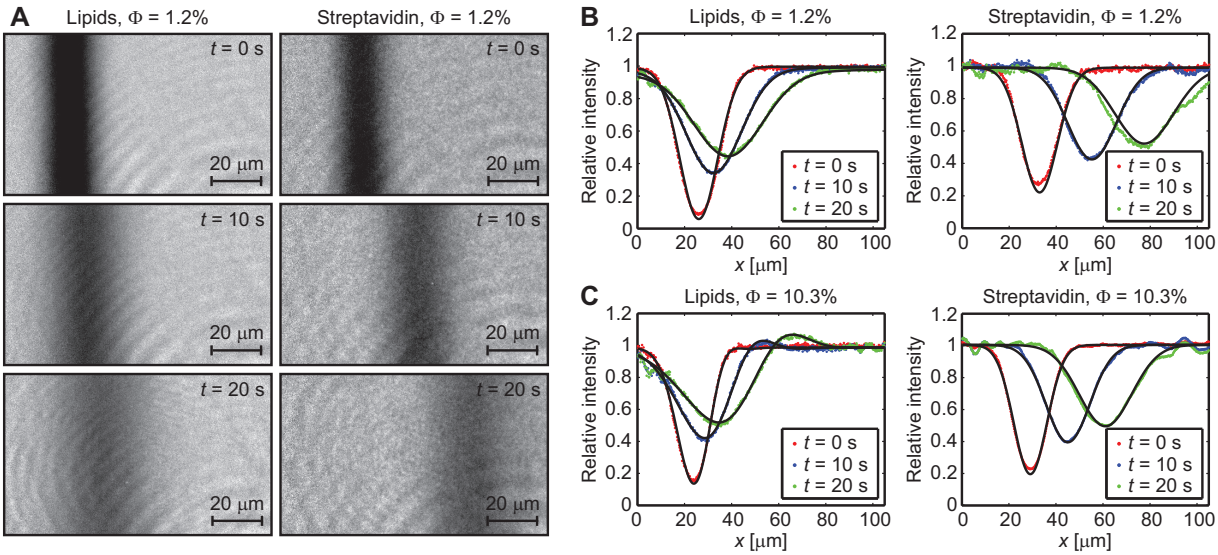

Figure 7. (A) Experimental data showing the fluorescence intensity from the lipid OG488-DHPE (left) and the anchored protein SA-647 (right) in an SLB after photobleaching at t = 0 s. There is a ~20 mL liquid flow from left to right in all images. The images are for a streptavidin coverage of Φ = 1.2%. **(B)** Corresponding line profiles obtained by averaging the intensity

perpendicular to the bleach line. **(C)** Intensity line profiles for a SA-647 surface coverage of Φ = 10.3%. The solid lines are curve fits to Eq. 10.

Table 2. Experimentally determined values of the drift velocity, $v_{\text{SA-647}}$, and the diffusivity, $D_{\text{SA-647}}$, of the protein SA-647 at different surface coverage, Φ. The corresponding drift velocities of the OG488-DHPE lipids, v_{lipids}, are also listed. The values are presented as mean value ± one standard deviation from 3 to 7 measurements (5 to 7 measurements for the drift velocity experiments). The diffusivity from measurements without flow is indicated with the index "no flow", and the columns $v_{\text{c,exp}}$ and $v_{\text{c,sim}}$ is the relative drift velocity, $v_c = v_{\text{SA-647}} - v_{\text{lipids}}$, from the experiments and from the hydrodynamic force simulations, respectively.

	Φ = 1.2%	**Φ = 5.7%**	**Φ = 10.3%**
v_{lipids} **[µm/s]**	0.67 ± 0.05	0.67 ± 0.04	0.58 ± 0.06
$v_{\text{SA-647}}$ **[µm/s]**	2.20 ± 0.06	1.76 ± 0.06	1.53 ± 0.04
$v_{\text{c,exp}}$ **[µm/s]**	1.53 ± 0.08	1.09 ± 0.07	0.95 ± 0.07
$v_{\text{c,sim}}$ **[µm/s]**	1.47	1.07	0.84
$D_{\text{SA-647}}$ **[µm^2/s]**	1.13 ± 0.09	0.91 ± 0.04	0.95 ± 0.04
$D_{\text{SA-647,no flow}}$ **[µm^2/s]**	1.08 ± 0.09	0.96 ± 0.02	0.95 ± 0.01

To compare the experimental data with the results from the simulations, the bound streptavidin molecule is modeled as a cylinder with a = 3 nm and h_c = 5 nm.[36] Using Eq. 12, this gives a value of $A_{\text{hydro}}(0)$ = 315 nm^2, and from Eq. 14 $A_{\text{hydro}}(1.2\%)$ = 306 nm^2, $A_{\text{hydro}}(5.7\%)$ = 251 nm^2, and $A_{\text{hydro}}(10.3\%)$ = 199 nm^2. Inserted into Eq. 19, with A_m = 0, T = 295 K, σ_{hydro} = 18.1 Pa, and D_c given by $D_{\text{SA-647,no flow}}$ in Table 2, for each surface coverage this gives the value $v_{\text{c,sim}}$, which is within 4% of the experimentally determined relative drift velocity at Φ = 1.2% and Φ = 5.7% and within 12% at Φ = 10.3%. However, the agreement with theory for the latter surface

coverage is within 3% if the drift velocity for the lipids obtained at $\Phi = 1.2\%$ and $\Phi = 5.7\%$ is used instead of 0.58 μm/s. The hydrodynamic length, d_{hydro}, is under these conditions around 1 μm, and a significant redistribution of streptavidin can thus be expected for any lipid bilayer enclosure larger than 1 μm.

The drift velocity of the lipids in the channel was similar at the three surface coverages. This value can also be used to estimate the intermonolayer friction coefficient, b, which with v_{lipids} = 0.67 μm/s gives $b = 2.7\times10^7$ Pa·s/m, of similar magnitude as the value $b = 2.4\times10^7$ Pa·s/m determined previously by Jönsson et al.[23]

The diffusivity obtained for SA-647 in the flow experiments is similar to the values obtained from measurements without flow. The diffusivity drops slightly for the higher surface coverage compared to the diffusivity at low coverage, likely due to obstruction effects between the streptavidin molecules. The diffusivity of the lipids was determined to 2 to 3 $\mu m^2/s$.

The data in Figure 7 indicate that the hydrodynamic force determined from the simulations is in good agreement with experimental values. The drift velocity might be different for different situations, for example for situations where Eq. 19 does not hold; however, the hydrodynamic force on an individual protruding macromolecule is expected to be similar.

How does these results compare with the existing values in the literature? There is a lack of detailed drift velocity and diffusivity measurements as provided here, but Engstler et al. measured quantitatively the transport of different protein complexes anchored to the mobile surface coat of the parasite *Trypanosoma brucei* due to hydrodynamic forces when the parasite is swimming.[7] Comparison with proteins of different size showed that larger proteins where transported more rapidly than smaller proteins. Bound IgG had a half-life clearance to the posterior pole of the cell that was, at least, 5 times faster than that of the smaller protein

streptavidin coupled to the same surface coat. Modeling IgG as a spherical particle with a radius of 7.5 nm,[7] and streptavidin as a cylinder with a = 3 nm and h_c = 5 nm,[36] and using $A_{hydro}(0) = 10.2\pi a^2$ for a spherical molecule and Eqs. 12 and 14 leads to $F_{hydro}(IgG)/F_{hydro}(streptavidin) = 5$ at the surface concentrations stated by Engstler et al.: $\Phi(IgG) \approx 0.5\% \times (7.5/2.5)^2 = 4.5\%$ and $\Phi(streptavidin) \approx 1\% \times (3/2.5)^2 = 1.4\%$. If the diffusivities of the two protein complexes on the surface are comparable in magnitude, this means that IgG will have a velocity ~5 times higher than streptavidin (see Eq. 19), in agreement with the experimental observations. We have also previously used hydrodynamic trapping of streptavidin molecules bound to an SLB to estimate the effect of hydrodynamic shielding at different surface coverage.[25] These experiments gave a decrease in A_{hydro} of 23% going from Φ = 11% to Φ = 16% and a decrease of 11% in A_{hydro} going from Φ = 16% to Φ = 19%. This can be compared to a decrease of 21% going from Φ = 11% to Φ = 16% and a decrease of 12% going from Φ = 16% to Φ = 19%, when using Eq. 14 with the previously stated values for streptavidin, which is of similar magnitude as the experimental results. However, it should be noted that at these high surface coverages there are also significant intermolecular interactions between streptavidin molecules which will affect the apparent value of A_{hydro} determined from the hydrodynamic trapping experiments. Thus, even though A_{hydro} changes with Φ as expected from theory, the absolute values for A_{hydro} from the hydrodynamic trapping experiments will appear lower due to intermolecular repulsion.[25] This effect is avoided when performing the measurements at constant surface coverage as done in this work, which allows us to measure only the hydrodynamic force.

CONCLUSIONS

A constant liquid flow outside a cell surface can cause mobile macromolecules that are anchored in the lipid bilayer to move in the direction of the flow. This transport results in a redistribution of macromolecules in the lipid bilayer. The hydrodynamic force that acts on each macromolecule is proportional to the macroscopic shear stress on the cell surface, σ_{hydro}, which is a macroscopic parameter that is independent of the properties of the protruding molecules in the lipid bilayer. The proportionality constant, A_{hydro}, is a parameter corresponding to the effective hydrodynamic area of the macromolecule, which will depend on both the size and shape of the studied molecule as well as the surface coverage of these molecules. The hydrodynamic force acting on a cylindrical molecule will at low coverage increase with the size of the molecule according to Eq. 12, which generally results in taller molecules moving with a higher velocity than shorter molecules. The molecules will start to shield each other from the hydrodynamic flow at higher surface coverage (see Eq. 14). This typically starts to happen at a coverage $\Phi \sim \pi a^2/A_{\text{hydro}}(0)$, which is the ratio between the cross-sectional area of the molecule and the effective hydrodynamic area of the molecule at low surface coverage.

For the experiments in this study we have shear stresses on the order of 10 Pa acting on the lipid bilayer, which results in a net drift velocity of the ~5 nm large, anchored protein streptavidin of approximately 1 μm/s in the direction of the flow. The value 10 Pa is also a typical shear stress on the floor of a microfluidic channel with a cross-sectional area of 100 μm × 100 μm when exposed to a liquid flow of 100 μL/min.[23] As a comparison, the shear stress on the wall of blood arteries due to blood flow is of the order of 1 Pa,[37] which is of similar magnitude as the shear stress on the surface of a swimming parasite in a blood capillary[7]. Since it is the shear stress that determines the hydrodynamic force for a specific macromolecule, this indicates that

liquid flows can have a significant effect on the redistribution of membrane-anchored macromolecules in vitro as well as in vivo.

Knowing how the magnitude of the hydrodynamic force depends on the size and coverage of molecules in the lipid bilayer opens up for several interesting applications. One is to use this knowledge to determine the interaction between molecules in a lipid bilayer using hydrodynamic trapping.[25] By relating the hydrodynamic force from a liquid flow out of a pipette to the accumulation of macromolecules in a lipid bilayer makes it possible to measure the force between these molecules as a function of intermolecular distance.

An interesting observation is the strong dependence the size of the studied molecules has on the hydrodynamic force. For model systems such as SLBs the ability to predict the hydrodynamic force on different types of molecules in the lipid bilayer can open up for detailed studies of the diffusivity of different populations of molecules based on Eq. 19 or to design conditions to be able to separate different types of membrane-associated molecules based on size. It can also explain how liquid flows can change the concentration of membrane-associated molecules on the surface of a cell.

Overall, this new type of information could help in understanding how molecules on the surface of cells interact and also be used to better characterize and understand membrane protein separation and redistribution in lipid bilayers.

Supporting Information

Three supporting figures showing: (i) simulated values of the shear stress acting on a lipid bilayer beneath an absorbed spherical molecule, and (ii-iii) simulated values of the magnitude of the local velocity field and the local pressure distribution for molecules of different shape at low

coverage and at $\Phi = 0.1$. One supporting table listing simulated values for $A_{hydro}/\pi a^2$ at different surface coverage and molecular shapes. Supporting text containing derivations of the creeping flow equations. This material is available free of charge on the ACS Publications website at DOI: 10.1021/acs.langmuir.5b03421.

Acknowledgment

This work was supported by grants from the Swedish Research Council (number: 623-2014-6387 and 621-2014-3907).

REFERENCES

(1) Singer, S. J.; Nicolson, G. L. The Fluid Mosaic Model of the Structure of Cell Membranes. *Science* **1972**, *175*, 720–731.

(2) Vereb, G.; Szöllosi, J.; Matkó, J.; Nagy, P.; Farkas, T.; Vigh, L.; Mátyus, L.; Waldmann, T. A.; Damjanovich, S. Dynamic, yet Structured: The Cell Membrane Three Decades after the Singer-Nicolson Model. *Proc. Natl. Acad. Sci. U. S. A.* **2003**, *100*, 8053–8058.

(3) Saffman, P. G.; Delbrück, M. Brownian Motion in Biological Membranes. *Proc. Natl. Acad. Sci. U. S. A.* **1975**, *72*, 3111–3113.

(4) Levine, A. J.; Liverpool, T. B.; MacKintosh, F. C. Dynamics of Rigid and Flexible Extended Bodies in Viscous Films and Membranes. *Phys. Rev. Lett.* **2004**, *93*, 038102–1.

(5) Evans, E.; Sackmann, E. Translational and Rotational Drag Coefficients for a Disk Moving in a Liquid Membrane Associated with a Rigid Substrate. *J. Fluid Mech.* **1988**, *194*, 553.

(6) Türkcan, S.; Richly, M. U.; Bouzigues, C. I.; Allain, J.-M.; Alexandrou, A. Receptor

Displacement in the Cell Membrane by Hydrodynamic Force Amplification through Nanoparticles. *Biophys. J.* **2013**, *105*, 116–126.

(7) Engstler, M.; Pfohl, T.; Herminghaus, S.; Boshart, M.; Wiegertjes, G.; Heddergott, N.; Overath, P. Hydrodynamic Flow-Mediated Protein Sorting on the Cell Surface of Trypanosomes. *Cell* **2007**, *131*, 505–515.

(8) Castellana, E. T.; Cremer, P. S. Solid Supported Lipid Bilayers: From Biophysical Studies to Sensor Design. *Surf. Sci. Rep.* **2006**, *61*, 429–444.

(9) McConnell, H. M.; Watts, T. H.; Weis, R. M.; Brian, A. A. Supported Planar Membranes in Studies of Cell-Cell Recognition in the Immune System. *Biochim. Biophys. Acta* **1986**, *864*, 95–106.

(10) Sackmann, E. Supported Membranes: Scientific and Practical Applications. *Science* **1996**, *271*, 43–48.

(11) Johansson, B.; Olsson, T.; Jönsson, P.; Höök, F. Hydrodynamic Separation of Proteins in Supported Lipid Bilayers Confined by Gold Barriers. *Soft Matter* **2013**, *9*, 9414.

(12) Jönsson, P.; Beech, J. P.; Tegenfeldt, J. O.; Höök, F. Shear-Driven Motion of Supported Lipid Bilayers in Microfluidic Channels. *J. Am. Chem. Soc.* **2009**, *131*, 5294–5297.

(13) Simonsson, L.; Gunnarsson, A.; Wallin, P.; Jönsson, P.; Höök, F. Continuous Lipid Bilayers Derived from Cell Membranes for Spatial Molecular Manipulation. *J. Am. Chem. Soc.* **2011**, *133*, 14027–14032.

(14) Jönsson, P.; Jonsson, M. P.; Höök, F. Sealing of Submicrometer Wells by a Shear-Driven Lipid Bilayer. *Nano Lett.* **2010**, *10*, 1900–1906.

(15) Chao, L.; Richards, M. J.; Hsia, C.-Y.; Daniel, S. Two-Dimensional Continuous Extraction in Multiphase Lipid Bilayers to Separate, Enrich, and Sort Membrane-Bound Species. *Anal. Chem.* **2013**, *85*, 6696–6702.

(16) Ainla, A.; Gözen, I.; Hakonen, B.; Jesorka, A. Lab on a Biomembrane: Rapid Prototyping and Manipulation of 2D Fluidic Lipid Bilayers Circuits. *Sci. Rep.* **2013**, *3*, 2743.

(17) Jönsson, P.; Gunnarsson, A.; Höök, F. Accumulation and Separation of Membrane-Bound Proteins Using Hydrodynamic Forces. *Anal. Chem.* **2011**, *83*, 604–611.

(18) Granéli, A.; Yeykal, C. C.; Prasad, T. K.; Greene, E. C. Organized Arrays of Individual DNA Molecules Tethered to Supported Lipid Bilayers. *Langmuir* **2006**, *22*, 292–299.

(19) Frykholm, K.; Freitag, C.; Persson, F.; Tegenfeldt, J. O.; Granéli, A. Probing Concentration-Dependent Behavior of DNA-Binding Proteins on a Single-Molecule Level Illustrated by Rad51. *Anal. Biochem.* **2013**, *443*, 261–268.

(20) Goldman, A. J.; Cox, R. G.; Brenner, H. Slow Viscous Motion of a Sphere Parallel to a Plane wall—II Couette Flow. *Chem. Eng. Sci.* **1967**, *22*, 653–660.

(21) O'Neill, M. E. A Sphere in Contact with a Plane Wall in a Slow Linear Shear Flow. *Chem. Eng. Sci.* **1968**, *23*, 1293–1298.

(22) Chaoui, M.; Feuillebois, F. Creeping Flow around a Sphere in a Shear Flow Close to a Wall. *Q. J. Mech. Appl. Math.* **2003**, *56*, 381–410.

(23) Jönsson, P.; Beech, J. P.; Tegenfeldt, J. O.; Höök, F. Mechanical Behavior of a Supported Lipid Bilayer under External Shear Forces. *Langmuir* **2009**, *25*, 6279–6286.

(24) Honerkamp-Smith, A. R.; Woodhouse, F. G.; Kantsler, V.; Goldstein, R. E. Membrane Viscosity Determined from Shear-Driven Flow in Giant Vesicles. *Phys. Rev. Lett.* **2013**, *111*, 1–5.

(25) Jönsson, P.; McColl, J.; Clarke, R. W.; Ostanin, V. P.; Jönsson, B.; Klenerman, D. Hydrodynamic Trapping of Molecules in Lipid Bilayers. *Proc. Natl. Acad. Sci. U. S. A.* **2012**, *109*, 10328–10333.

(26) Leal, L. G. *Laminar Flow and Convective Transport Processes*; Butterworth-Heinemann, New York, 1992.

(27) Happel, J.; Brenner, H. *Low Reynolds Number Hydrodynamics*; Martinus Nijhoff, Cambridge, 1983.

(28) Edelstein, A. D.; Tsuchida, M. A.; Amodaj, N.; Pinkard, H.; Vale, R. D.; Stuurman, N. Advanced Methods of Microscope Control Using μManager Software. *J. Biol. Methods* **2014**, *1*, 1–10.

(29) Jönsson, P.; Jonsson, M. P.; Tegenfeldt, J. O.; Höök, F. A Method Improving the Accuracy of Fluorescence Recovery after Photobleaching Analysis. *Biophys. J.* **2008**, *95*, 5334–5348.

(30) Atkins, P. W. *Physical Chemistry*; 5th ed.; Oxford University Press, Oxford, 1997.

(31) Jacobson, K.; Ishihara, A.; Inman, R. Lateral Diffusion of Proteins in Membranes. *Annu. Rev. Physiol.* **1987**, *49*, 163–175.

(32) Ramadurai, S.; Holt, A. Lateral Diffusion of Membrane Proteins. *J. Am. Chem. Soc.* **2009**, *131*, 12650–12656.

(33) Reits, E. A.; Neefjes, J. J. From Fixed to FRAP: Measuring Protein Mobility and Activity in Living Cells. *Nat. Cell Biol.* **2001**, *3*, E145–E147.

(34) Macháň, R.; Hof, M. Lipid Diffusion in Planar Membranes Investigated by Fluorescence Correlation Spectroscopy. *Biochim. Biophys. Acta, Biomembr.* **2010**, *1798*, 1377–1391.

(35) Jönsson, P.; Höök, F. Effects of Surface Pressure and Internal Friction on the Dynamics of Shear-Driven Supported Lipid Bilayers. *Langmuir* **2011**, *27*, 1430–1439.

(36) Darst, S. A.; Ahlers, M.; Meller, P. H.; Kubalek, E. W.; Blankenburg, R.; Ribi, H. O.; Ringsdorf, H.; Kornberg, R. D. Two-Dimensional Crystals of Streptavidin on Biotinylated Lipid Layers and Their Interactions with Biotinylated Macromolecules. *Biophys. J.* **1991**, *59*, 387–396.

(37) Potters, W. V.; Marquering, H. A.; VanBavel, E.; Nederveen, A. J. Measuring Wall Shear Stress Using Velocity-Encoded MRI. *Curr. Cardiovasc. Imaging Rep.* **2014**, *7*, 1–12.

SUPPORTING INFORMATION

Hydrodynamic forces on macromolecules protruding from lipid bilayers due to external liquid flows

Peter Jönsson* and Bengt Jönsson[‡]

Division of Physical Chemistry, Lund University, SE-22100 Lund, Sweden
[‡]Department of Biophysical Chemistry, Lund University, SE-22100 Lund, Sweden

*Correspondence: peter.jonsson@fkem1.lu.se

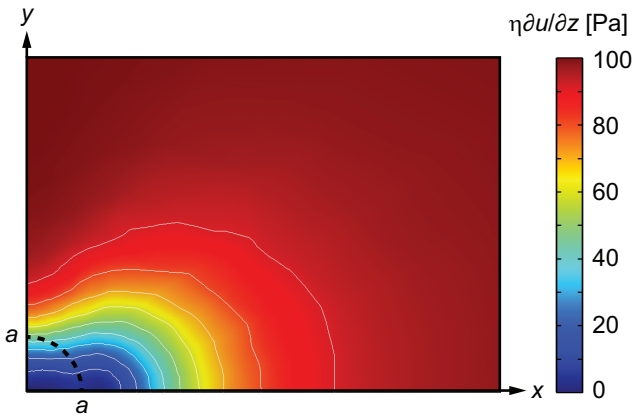

Figure S1. Simulated values of the shear stress acting on the membrane surface below the adsorbed spherical molecule (black dashed line) at a surface coverage of $\Phi = 0.001$. The magnitude of the shear stress without the absorbed molecule is $\sigma_{hydro} = 100$ Pa and the white lines correspond to contours of constant shear stress.

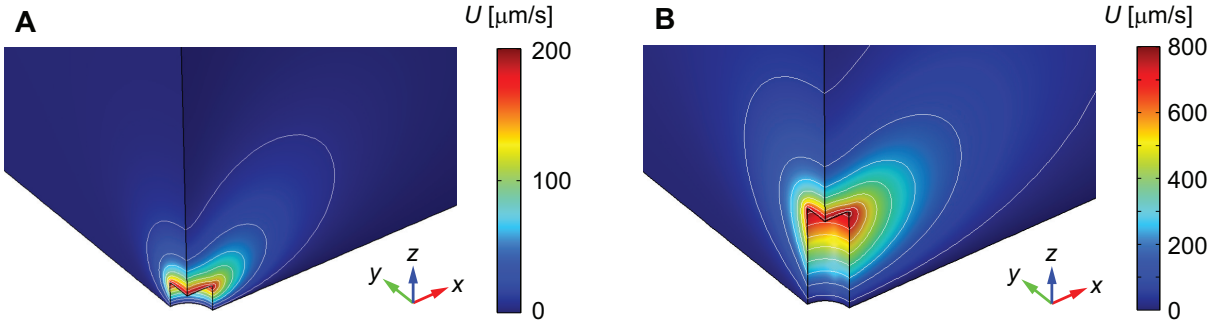

Figure S2. Simulated values of the magnitude of the local velocity field, $U = (u^2 + v^2 + w^2)^{0.5}$ around a cylindrical molecule with **(A)** $h_c = a$ and **(B)** $h_c = 4a$ at a surface coverage $\Phi = 0.001$. The white lines show contours of constant local velocity. The net flow above the molecule is in the x-direction.

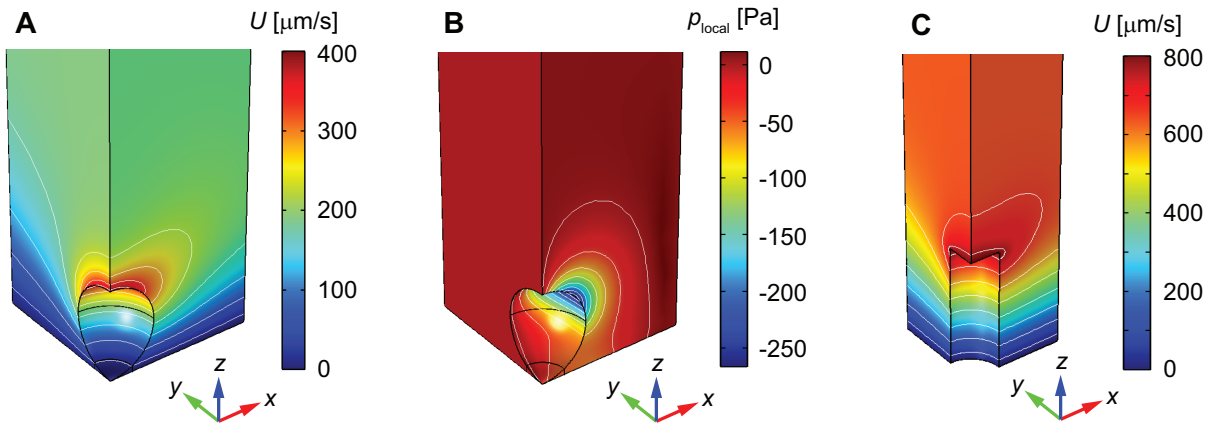

Figure S3. Simulated values of the magnitude of **(A)** the local flow velocity, $U = (u^2 + v^2 + w^2)^{0.5}$ and **(B)** the local pressure for a system with $\Phi = 0.1$. **(C)** The velocity magnitude for a cylindrical molecule with $h_c = 4a$ at $\Phi = 0.1$. The while lines shows contours of constant local velocity and pressure, respectively.

Table S1. Simulated values of $A_{hydro}/\pi a^2$ at some different surface coverage, Φ, for a cylindrical molecule with different height-to-width ratios, $h_c/2a$, and for a spherical molecule.

Φ	$h_c = a/2$	$h_c = a$	$h_c = 2a$	$h_c = 3a$	$h_c = 4a$	$h_c = 6a$	$h_c = 8a$	Sphere
0[a]	3.67	6.56	13.5	21.8	31.6	54.9	82.8	10.2
0.001	3.67	6.55	13.4	21.7	31.2	53.7	80.0	10.2
0.01	3.66	6.50	13.1	20.4	28.0	42.7	55.5	9.99
0.05	3.57	6.03	10.4	13.5	15.7	18.0	19.1	8.47
0.1	3.41	5.30	7.66	8.77	9.33	9.79	9.94	6.68
0.2	3.02	4.00	4.67	4.88	4.95	4.99	5.00	4.41
0.3	2.61	3.06	3.27	3.32	3.33	3.33	3.33	3.18
0.4	2.24	2.42	2.49	2.50	2.50	2.50	2.50	2.46
0.5	1.91	1.98	2.00	2.00	2.00	2.00	2.00	1.99

[a] The value at $\Phi = 0$ is extrapolated from the simulated data.

CREEPING FLOW EQUATIONS

Navier-Stokes' equations will under creeping flow conditions be given by:[1]

$$0 = -\nabla p + \eta \nabla^2 \boldsymbol{u} \tag{S1}$$

where $\boldsymbol{u}$ is the flow velocity vector and p the pressure. This equation can be used together with the equation of continuity, see Eq. S2, to describe steady state creeping flow in an incompressible fluid.

$$\nabla \cdot \boldsymbol{u} = 0 \tag{S2}$$

To model the flow around randomly adsorbed macromolecules on, or near, a lipid bilayer surface at $z = 0$ it is convenient to divide the flow velocity into two parts:

$$\boldsymbol{u} = \boldsymbol{u}_{\text{macro}} + \boldsymbol{u}_{\text{local}} \tag{S3}$$

where

$$\boldsymbol{u}_{\text{macro}} = \boldsymbol{u}_{\text{lipids}} + \left(\sigma_{\text{hydro}} z / \eta\right) \boldsymbol{e}_x \tag{S4}$$

The quantity σ_{hydro} is the shear stress on the plane surface at $z = 0$ without any absorbed molecules, which here is assumed to be in the x-direction ($\boldsymbol{e}_x$ is a unit vector in the direction of the flow), and $\boldsymbol{u}_{\text{lipids}}$ is the velocity of the lipid bilayer (which on the local length scale is assumed to be constant). Similarly, the pressure can also be divided up into a slowly varying macroscopic part and a local part varying on the length scale of the size of the absorbed molecules:

$$p = p_{\text{macro}} + p_{\text{local}} \tag{S5}$$

From Eq. S1 and Eq. S4 it can furthermore be observed that:

$$O\left(\nabla p_{\text{macro}}\right) = \sigma_{\text{hydro}} / d_{\text{macro}} << O\left(\nabla p_{\text{micro}}\right) = \sigma_{\text{hydro}} / a \tag{S6}$$

where d_{macro} is the length scale over which the global pressure changes (for example the width or height of the channel used in microfluidic experiments,[2] the size of a cell for in vivo experiment,[3] or the distance between the tip of a pipette and the membrane surface for hydrodynamic trapping experiments[4]), and a is the radius of the studied macromolecule. Inserted into Eqs. S1 and S2 this gives the creeping flow equations for the local flow:

$$0 = -\nabla p_{\text{local}} + \eta \nabla^2 \boldsymbol{u}_{\text{local}} \tag{S7}$$

$$\nabla \cdot \boldsymbol{u}_{\text{local}} = 0 \tag{S8}$$

The benefit of using p_{local} and $\boldsymbol{u}_{\text{local}}$ is that these quantities approaches zero when moving away from the adsorbed molecules on the surface, which simplifies the simulations. The hydrodynamic drag force on a part of the molecule with the area dA and the unit normal $\boldsymbol{n} = (n_x, n_y, n_z)$ is:[1]

$$dF_x = \left(p_{\text{local}} - 2\eta \frac{\partial u}{\partial x} \right) n_x dA - \eta \left(\frac{\partial u}{\partial y} + \frac{\partial v}{\partial x} \right) n_y dA - \eta \left(\frac{\partial u}{\partial z} + \frac{\partial w}{\partial x} \right) n_z dA - \sigma_{\text{hydro}} n_z dA \tag{S9}$$

where the local velocity of the liquid is written $\boldsymbol{u}_{\text{local}} = (u, v, w)$. The total hydrodynamic drag force, F_{hydro}, is obtained by integrating dF_x over the surface of the molecule. Note also that F_{hydro} is independent on the velocity of the lipid bilayer, as long as Eq. S4 holds. From Eq. S7 and the definition of $\boldsymbol{u}_{\text{macro}}$ in Eq. S4 it follows that both $\boldsymbol{u}_{\text{local}}$ and p_{local} scales linearly with σ_{hydro}. Furthermore, the hydrodynamic force will be proportional to a^2 for two molecules on

the surface with the same shape and the same surface coverage, but with different size. Thus, it is sufficient to perform the simulations for one hydrodynamic shear stress, and one size of the molecules, only.

SUPPORTING REFERENCES

(1) Leal, L. G. *Laminar Flow and Convective Transport Processes*; Butterworth-Heinemann, New York, 1992.

(2) Jönsson, P.; Gunnarsson, A.; Höök, F. Accumulation and Separation of Membrane-Bound Proteins Using Hydrodynamic Forces. *Anal. Chem.* **2011**, *83* (2), 604–611.

(3) Engstler, M.; Pfohl, T.; Herminghaus, S.; Boshart, M.; Wiegertjes, G.; Heddergott, N.; Overath, P. Hydrodynamic Flow-Mediated Protein Sorting on the Cell Surface of Trypanosomes. *Cell* **2007**, *131* (3), 505–515.

(4) Jönsson, P.; McColl, J.; Clarke, R. W.; Ostanin, V. P.; Jönsson, B.; Klenerman, D. Hydrodynamic Trapping of Molecules in Lipid Bilayers. *Proc. Natl. Acad. Sci. U. S. A.* **2012**, *109* (26), 10328–10333.